Dynamics of an Adaptive Hybrid

William A. Sethares, *Member, IEEE*, and Iven M. Y. Mareels, *Member, IEEE*

Abstract—**Adaptive hybrids are one way of canceling the echo path in telephone systems. This paper conducts a bifurcation analysis of a simplified model of an adaptive hybrid using two bifurcation parameters, the adaptive stepsize and the ratio of the two inputs. As these parameters vary, the system exhibits a wide variety of behaviors, including stable and unstable equilibrium points, stable and unstable periodic orbits, and aperiodic orbits. The underlying bifurcations include Hopf, flip, period doubling sequences, and a degenerate global bifurcation which gives rise to some very complex dynamics. For inputs with a spectral density, conditions are derived under which a single stable (averaged) equilibrium exists.**

These results have two interesting points of view. From the practical side, they provide an explanation of the intermittent bursting behavior of adaptive hybrids, demonstrating that bursting can be due to a slowly attractive periodic orbit (in which case the bursting eventually dies away), to a stable aperiodic orbit, or to a strange attractor (in which cases the bursting persists). From the theoretical side, these results are interesting because they provide a "real world" example exhibiting a rich variety of nonlinear behaviors. Due to the particular form of the model, many of these behaviors can actually be proven.

I. Introduction

A DEVICE called a "4:2 hybrid" is used in telephone systems to transform the four-wire long distance receive and transmit lines to and from a two-wire local line. An ideal hybrid would move all the incoming signal from the four-wire receive line to the two-wire local line, and simultaneously move the outgoing signals from the two-wire local line to the four-wire transmit line. In a real device, however, some of the energy in the incoming line will inevitably leak into the outgoing line. One solution, called adaptive echo cancelation [1], uses an adaptive filter to match, or identify, the dynamics of the leakage path (see Fig. 1). When the near end speaker is silent, and when the adaptive filter has matched the transfer function of the hybrid, $\hat{y}$ will equal y, their difference is zero, and the echo of the far end speech is canceled. The adaptive solution to the hybrid problem is well established, and has been used successfully in a wide variety of situations [2].

1.1. Problem Description

In certain situations, however, an intermittent "bursting" or "chirping" or "bumping" misbehavior arises. This was first brought to our attention [17] by a series of laboratory tests at Tellabs Inc. which were designed to investigate the adaptive hybrid system when the received signal is significantly correlated with the near end signal within the time

Manuscript received October 23, 1989; revised May 18, 1990. This paper was recommended by Associate Editor D. Graupe.

W. A. Sethares is with the Department of Electrical and Computer Engineering, University of Wisconsin, Madison, WI 53706.

I. M. Mareels is with the Department of Electrical and Computer Engineering, University of Newcastle, Newcastle, NSW, Australia 2308.

IEEE Log Number 9039215.

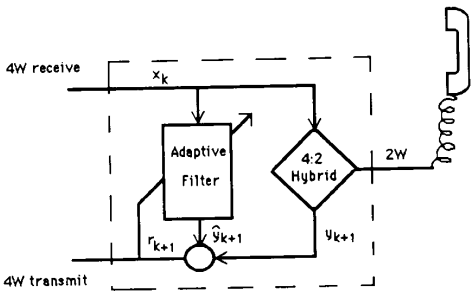

Fig. 1. Basic adaptive hybrid.

window of the adaptive filter. Such correlations become increasingly likely as the adaptive hybrid is used on communications lines of shorter length. The real time tests utilized a 20-tap adaptive hybrid at the near end of the line and a simple (nonadaptive) hybrid at the far end, giving 6-dB attenuation around the loop. Independent narrow-band modem signals were injected at each end. Long periods of close match between the output of the adaptive hybrid and the echo path were observed, and the hybrid appeared to be functioning well. Suddenly and with no warning, the system would begin "singing", the signals degenerated into wild oscillation, and then the system would quickly restabilize. These bursts were intermittent and had no apparent cause.

In [3], a simple model of the hybrid was introduced and it was shown that a similar bursting occurred in the model due to a lack of "persistent excitation" combined with the inherent feedback structure of the adaptive hybrid telephone system. The bursting cycle was characterized by a long linear drift phase, followed by large oscillations that quickly restabilize, returning again to the drift phase. It was conjectured that certain combinations of excitation might lead to chaotic behavior. This conjecture is examined in the present paper, and numerous nonlinear behaviors are revealed, some of which may occur in physically reasonable situations. The bursting is revealed to be either a region of stable aperiodic orbits, a marginally stable two periodic orbit or (perhaps) a strange attractor, depending on the relative magnitudes of the two inputs to the system, and depending on the adaptive stepsize parameter. Unravelling the behavior of this model leads to insights concerning how to avoid such bursting misbehaviors. One approach, using coded inputs, is suggested in [19].

The next subsection derives the model for the adaptive hybrid in the form of a two input, two state discrete mapping $\boldsymbol{F}$. The inputs represent the near and far end transmission, while the states are the loop gain and the received signal. The physical meaning of the bifurcation parameters μ (the

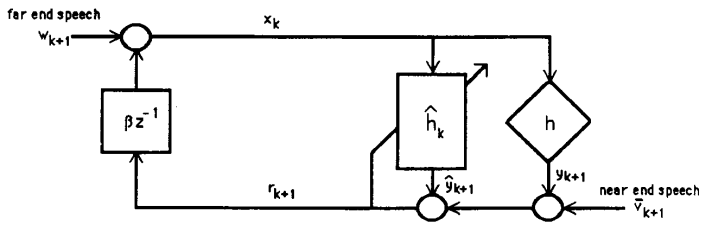

Fig. 2. Single adaptive hybrid.

adaptive stepsize) and α (the ratio of the inputs) are discussed, and the interpretation of α as a degree of excitation is proposed.

Under the simplifying assumption that the ratio of the two inputs is constant, Section II carries out a bifurcation analysis by finding the equilibria of F and examining their stability, and by finding the two periodic orbits and examining their stability. Several types of bifurcations are found, including Hopf, flip, and a degenerate global bifurcation. For large values of the bifurcation parameter, unwanted instabilities due to a "large stepsize" are encountered. These are overcome by a reparameterization of F that allows the analysis to continue to α at infinity.

Section III analyzes the behavior of the adaptive hybrid model for more general inputs by defining an averaged equation which approximates the behavior of the real system under certain operating conditions. For inputs with a spectral density, a condition is derived which ensures the existence of a stable averaged operating point. The special case of sinusoidal inputs is examined concretely to give conditions on the magnitude and frequencies which ensure that this condition is fulfilled. Failing these conditions, the averaged equation (along with the hybrid itself) will leave the stability region, causing the bursting behavior.

Section IV presents extensive simulations and diagrams that comprehensively explain the adaptive hybrid system when excited by constant inputs. Combined with the analysis, these pictures allow a reasonable explanation of the bursting phenomenon as one of three possible behaviors, depending on the conditions under which the system operates. The final section presents our conclusions and relates this analysis to examinations of the "bursting" phenomena in other adaptive systems [4]–[7], [11]–[15].

1.2. Technical Formulation

The system will be modeled in the simplest possible manner as in [3]. A single parameter adaptive hybrid at the near end attempts to cancel the echo of the far end speech. At the far end, a (nonadaptive) hybrid is modeled as an attenuation β and a delay. Please refer to Fig. 2, where $\bar{v}_k / w_k$ represent the near/far end speech, h represents the echo path at the near end, and r_k / x_k represent the received/transmitted signals at the near end. The adaptive parameter $\hat{h}$ is updated with the standard least mean squares algorithm:

$$\hat{h}_{k+1} = \hat{h}_k + \mu' x_k r_{k+1} \tag{1.1}$$

where μ' is the adaptive stepsize. The transmitted signal, containing the near end speech, the leakage from the far end speech, and the output of the adaptive filter is

$$\begin{aligned} r_{k+1} &= y_{k+1} - \hat{y}_{k+1} + \bar{v}_{k+1} \\ &= hx_k - \hat{h}_k x_k + v_{k+1}. \end{aligned} \tag{1.2}$$

Introducing the parameter error $\tilde{h}_k = h - \hat{h}_k$ and substituting (1.2) into (1.1) yields

$$\tilde{h}_{k+1} = \tilde{h}_k - \mu' x_k^2 \tilde{h}_k - \mu' x_k \bar{v}_{k+1} \tag{1.3}$$

while x_k itself is composed of

$$\begin{aligned} x_{k+1} &= w_{k+1} + \beta r_{k+1} \\ &= \beta \tilde{h}_k x_k + \beta \bar{v}_{k+1} + w_{k+1}. \end{aligned} \tag{1.4}$$

The equation pair (1.3) and (1.4) is a two-state $(\tilde{h}_k, x_k)$ nonlinear equation with two inputs, $\bar{v}_k$ and w_k. With $v_k = \beta \bar{v}_k$ and $h_k = \beta \tilde{h}_k$, this is equivalent to the mapping F: $\boldsymbol{R}^2 \to \boldsymbol{R}^2$,

$$F\begin{pmatrix} y \\ h \end{pmatrix} = \begin{pmatrix} hy + v + w \\ h - \mu y^2 h - \mu v y \end{pmatrix}. \tag{1.5}$$

The analysis of (1.5) begins in Section II with a special case —a "dc" or steady-state analysis in which the inputs are held constant, and is then expanded via an averaging argument to consider more general inputs in section III.

Reparameterize (1.3)–(1.4) with $v_k = v$ and $w_k = w$ for every k. Let $\mu = \mu' / w^2$, $\alpha = \beta v / w$, $h_k = \beta \tilde{h}_k$, and $y_k = x_k / w$. The system is then

$$F\begin{pmatrix} y \\ h \end{pmatrix} = \begin{pmatrix} hy + \alpha + 1 \\ h - \mu y^2 h - \mu \alpha y \end{pmatrix}. \tag{1.6}$$

In (1.6), h and y represent the states of the system (h is the loop gain, y is the received signal), while μ and α are the bifurcation parameters. Physically, μ represents a scaled version of the stepsize of the adaptive algorithm, while α is proportional to the *ratio* of the power of the two constant inputs v and w. Since μ' of (1.1) is a parameter chosen by the system designer, and since an upper bound on v and w are dictated by the physical properties of the telephone system (size of wires, maximum voltage swings, etc.), the analysis focuses mainly on "small" μ. It appears that the large μ case will exhibit regions of period doubling leading to chaos much as the large stepsize adaptive regulator of [4] leads to such behavior, though we have not pursued a detailed analysis here.

The parameter α, however, has no such natural limitations on magnitude, since the ratio $\beta v / w$ can reasonably assume any real value, with small w corresponding to large α. Speaking imprecisely (but nonetheless reasonably), small α correspond to a high degree of persistence of excitation of the adaptive algorithm, while large α correspond to a low

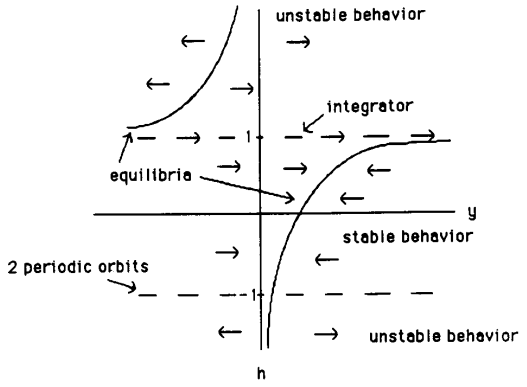

Fig. 3. Phase portrait behavior when $\mu = 0$.

degree of excitation. It is, of course, the latter which exhibit the more exotic (mis)behaviors. Since the excitation levels cannot generally be manipulated by the system designer, such exotic behaviors cannot be ruled out in applications.

II. Steady-State Analysis

Despite the apparent simplicity of the single parameter adaptive hybrid system (1.5), a complete analysis for all input pairs v_k and w_k is beyond the state of the art. A logical starting place is to consider the special case when the inputs are held constant as in (1.6). One many justify this simplification conceptually by supposing that the constants represent an averaged power of the inputs or one may recognize that an understanding of the behavior for general inputs requires an understanding for simple inputs. Even with this simplification, the behaviors exhibited by (1.6) are barely tractable. This section conducts a bifurcation analysis in the two variables μ and α (stepsize and ratio of the inputs), which proceeds by fixing μ and examining the behavior of the system for various values of α, and then by fixing α and studying the system as μ varies.

2.1. The $\mu = 0$ Case

The simplest version of (1.6) is when the adaptation is frozen with a zero stepsize. Though physically uninteresting, this case already exhibits some nontrivial behaviors. With $\mu = 0$, (1.6) becomes

$$\boldsymbol{F}\begin{pmatrix} y \\ h \end{pmatrix} = \begin{pmatrix} hy + \alpha + 1 \\ h \end{pmatrix}, \tag{2.1.1}$$

which has equilibria at $y^* = (\alpha + 1)/(1 - h^*)$ and h^* arbitrary ($h^* \neq 1$). This equilibrium is stable when $|h^*| < 1$ (though not asymptotically stable in the h direction) while it is unstable for $|h^*| > 1$. When $h^* = 1$, the map is a pure integrator and hence is unstable (except for the singular point $\alpha = -1$). At $h^* = -1$, (2.1.1) is again stable (though not asymptotically in either h or y).

For $h^* = -1$, there is also a family of stable 2 periodic orbits, since $y_{k+2} = y_k$. This information on the behavior of (2.1.1) is presented graphically in Fig. 3. Clearly, when h is allowed to vary by considering nonzero μ, the behavior of the system will be at least this complicated, involving both equilibria and periodic orbits.

2.2. Fixed-Point Analysis

A natural place to start the bifurcation analysis of $\boldsymbol{F}$ of (1.6) is to determine how the equilibria of the mapping change in response to different values of the adaptive stepsize μ and the ratio α. For $\alpha \neq -1$ and $\mu \neq 0$, $\boldsymbol{F}$ has a unique fixed point at

$$\begin{aligned} y^* &= 1 \\ h^* &= -\alpha. \end{aligned} \tag{2.2.1}$$

For $\alpha = -1$ there is an isolated fixed point at

$$\begin{aligned} y^* &= 1 \\ h^* &= 1 \end{aligned} \tag{2.2.2}$$

and a subspace of fixed points at

$$\begin{aligned} y^* &= 0 \\ h^* &\text{ arbitrary}. \end{aligned} \tag{2.2.3}$$

The stability of the isolated fixed points can be addressed by examining the eigenvalues of the Jacobian of $\boldsymbol{F}$, which is

$$D\boldsymbol{F}(y,h) = \begin{pmatrix} h & y \\ -2\mu yh - \mu\alpha & 1 - \mu y^2 \end{pmatrix}. \tag{2.2.4}$$

With y^* and h^* as in (2.2.1), $D\boldsymbol{F}(y^*, h^*)$ is

$$\begin{pmatrix} -\alpha & 1 \\ \mu\alpha & 1 - \mu \end{pmatrix} \tag{2.2.5}$$

which has characteristic equation

$$s^2 + (\alpha - 1 + \mu)s - \alpha. \tag{2.2.6}$$

Applying the Jury test for stability [10] shows that the magnitude of the roots of (2.2.6) (and hence the eigenvalues of (2.2.5)) are less than unity if and only if

$$\begin{aligned} \alpha &> -1 \\ \mu &> 0 \\ \alpha &< 1 - \mu/2 \end{aligned} \tag{2.2.7}$$

are satisfied simultaneously. This region is shaded in Fig. 4. All points on the boundary of this region are bifurcation points, since they represent values of α and/or μ for which the magnitude of the eigenvalues of (2.2.5) are exactly unity.

When $\mu = 0$, (2.2.5) reduces to an upper triangular matrix with diagonal elements 1 and $-\alpha$, indicating a global bifurcation. This is the vertical axis in Fig. 4.

For $\mu < 0$ and $\mu > 4$ there are no critical points and the system (1.6) is always unstable. These have simple physical explanations. Negative μ corresponds to a reversal of the sign of the adaptation gain, while $\mu > 4$ corresponds to instability induced by violation of the "small stepsize" requirement.

For $0 < \mu < 4$ there are exactly two critical points, at $\alpha = 1 - \mu/2$ and at $\alpha = -1$. When $\alpha = 1 - \mu/2$, (2.2.6) can be factored as $(s + 1)(s - 1 + \mu/2)$. The root at -1 indicates that these are *flip* bifurcations. We will see that these flips shed a two periodic orbit as $C2$ is crossed. The critical point where $\alpha = 1$ and $\mu = 0$ ($CP1$ of Fig. 4) is at the intersection of the line of global bifurcations C0 and the line of flip bifurcations $C2$. Thus $CP1$ is a degenerate flip bifurcation with eigenvalues 1 and -1.

The dynamics at the $\alpha = -1$ line are somewhat more involved. With y^* and h^* at the isolated fixed point of (2.2.2), the characteristic equation of the Jacobian is $s^2 +$

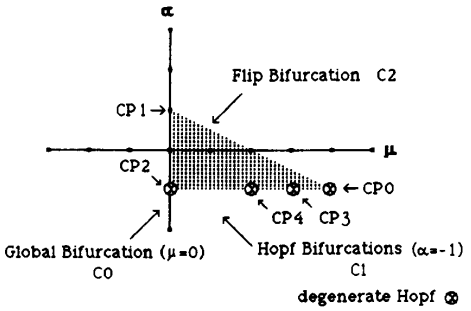

Fig. 4. Bifurcation diagram α versus μ.

$(-2+\mu)s+1$. This has roots at

$$s=\frac{2-\mu}{2}\pm\frac{i\sqrt{4\mu-\mu^2}}{2}$$

which have unity magnitude. Generically, this is a Hopf bifurcation with both eigenvalues on the unit circle for $0<\mu<4$. We will see later that this leads to a "circle" of aperiodic orbits for α close to but less than -1. As μ varies from 0 to 4, the roots move around the unit circle through the whole spectrum of possible Hopf bifurcations. Degeneracies occur at $\mu=0$ ($CP2$ with double 1 eigenvalue), at $\mu=2$ ($CP4$ with eigenvalues $+/-i$), at $\mu=3$ ($CP3$ with eigenvalues at $-0.5+/-i\sqrt{3}/2$), and at $\mu=4$ ($CP0$ with a double eigenvalue at -1). These critical points are degenerate Hopf bifurcations.

$CP0$ is a very special point. It sits at the intersections of the line of flip bifurcations and the line of Hopf bifurcations, and has two eigenvalues at -1. It is thus a Hopf and a flip and a global bifurcation all at once! The Jacobian of $\boldsymbol{F}$ at $CP0$ is

$$\boldsymbol{F}_{CP0}=\begin{pmatrix}1 & 1\\ -4 & -3\end{pmatrix}$$

which has only one eigenvector $(1,-2)$ and a generalized eigenvector $(-0.4,-0.2)$. Thus $CP0$ is a crucial point, an organizing center [13], and indicates the possibility of chaos in this neighborhood of parameter space.

2.3. Two-Periodic Analysis

There is a stable equilibrium only for values of α within the triangular region of Fig. 4, defined by (2.2.7). What happens outside this region where there are no stable equilibria? When there is a no stable fixed point, the next simplest possible behavior is that there might be low period orbits. The flip bifurcation indicates the existence of two-periodic orbits for systems whose parameters are above (but close to) the $C2$ line of Fig. 4. This is further enhanced by noting the existence of the two-period orbits in the frozen system ($\mu=0$ case). The search for two-periodic orbits can be pursued by noting that $\boldsymbol{F}^2$: $\boldsymbol{R}^2\to\boldsymbol{R}^2$ can be calculated directly from (1.5) as

$$\boldsymbol{F}^2\begin{pmatrix}y\\ h\end{pmatrix}=\begin{pmatrix}yh^2+(1+\alpha)(h+1)-\mu y(yh+1+\alpha)(yh+\alpha)\\ h-\mu\big(y^2h+y\alpha+\alpha(yh+1+\alpha)+h(yh+1+\alpha)^2\big)+\mu^2y(yh+1+\alpha)^2y(yh+\alpha)\end{pmatrix}. \tag{2.3.1}$$

This section focuses on the small stepsize case when $0<\mu\ll 1$, allowing us to locate periodic orbits to within $O(\mu)$ (or better) when exact expressions are forbidding. Pictorally, the analysis concentrates on the thin slice of Fig. 4 near the vertical axis. This small stepsize region represents the normal operating region of the adaptive hybrid system.

Period 2 orbits of (1.5) are the fixed points of (2.3.1). Of course, (2.2.1)–(2.2.3) are all fixed points, but are there others? At equilibrium, and assuming that $y(h-1)+(1+\alpha)\neq 0$ (which would yield a fixed point instead of a two periodic orbit), this term can be canceled from the first line of (2.3.1), yielding

$$h=-1+O(\mu). \tag{2.3.2}$$

This is not surprising. For $\mu=0$, $h=-1$ gives rise to a two-periodic orbit. (2.3.2) shows that some of these orbits persist for nonzero μ. Substituting (2.3.2) into the second line of (2.3.1), and looking for equilibria gives

$$y^2-(1+\alpha)y+\frac{(1+\alpha)}{2}+O(\mu^2)=0. \tag{2.3.3}$$

This can be solved to within $O(\mu)$ using the quadratic formula:

$$y=\frac{1+\alpha}{2}\pm\frac{\sqrt{\alpha^2-1}}{2}. \tag{2.3.4}$$

Assuming that $-1<\alpha<1-\mu/2$, the solution is imaginary, indicating that there is no two periodic orbit. For $|\alpha|>1$, (the region of interest, for which the equilibria are unstable), the two solutions to (2.3.4) are real. Designate these solutions y_1 and y_2. Then the corresponding h_1 and h_2 are

$$\begin{aligned}h_1&=-1+b_1\mu+O(\mu^2)\\ h_2&=-1+b_2\mu+O(\mu^2)\end{aligned} \tag{2.3.5}$$

where b_1 and b_2 are determined by substituting the h_i values of (2.3.5) into the first line of (2.3.1). This gives

$$\begin{aligned}b_1&=\frac{y_1(y_1-\alpha)(y_1-1-\alpha)}{1+\alpha-2y_1}\\ b_2&=\frac{y_2(y_2-\alpha)(y_2-1-\alpha)}{1+\alpha-2y_2}.\end{aligned} \tag{2.3.6}$$

The corresponding two-periodic trajectory alternates between (h_1,y_1) and (h_2,y_2) to within $O(\mu^2)$ for h an to within $O(\mu)$ for y. To make this somewhat more concrete, consider the following.

Example 1: With $\alpha=1.2$ and $\mu=0.01$, $y_1=1.4316$, $y_2=0.7683$, and hence $b_1=0.38417$, and $b_2=0.71583$. The parameters h_1 and h_2 are then -0.99616 and -0.99284. Simulating (1.5) directly (or simulating (1.3)–(1.4) with appropriate substitutions), and waiting 50000 iterations leads to the two-periodic solution $(-0.9962, 1.4395)$ and $(-0.9928, 0.7660)$. Note that all numbers are within the prescribed accuracy.

Example 2: With $\alpha=-1.2$ and $\mu=0.01$, $y_1=0.2317$, $y_2=-0.4317$, $b_1=-0.2158$, $b_2=0.1158$, and h_1 and h_2 can be calculated as -1.002158 and -0.9988417. Simulating (1.5)

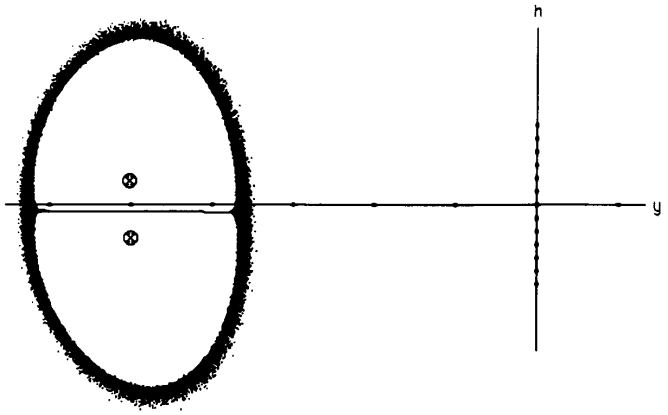

Fig. 5. $\alpha = -1.2$.

directly, with this value of α, the simulation does not settle into a two-periodic orbit even after 25 million iterations! See Fig. 5.

The stability of the two-period map can be determined by the eigenvalues of the Jacobian of the two iteration map. Since $DF^2(y_2,h_2) = DF(y_1,h_1)DF(y_2,h_2)$, this is

$$\begin{pmatrix} 1-\mu(b_1+b_2)+2\mu y_1 y_2-\mu\alpha y_1 & y_1-y_2+\mu b_1 y_2-\mu y_1 y_2^2 \\ -2\mu y_1+2\mu y_2 & 1-\mu(y_1^2+y_2^2)+2\mu y_1 y_2-\mu\alpha y_2 \end{pmatrix} + O(\mu^2). \tag{2.3.7}$$

The characteristic polynomial of (2.3.7) may be expressed as $s^2 + a_1 s - a_2$ where

$$\begin{aligned} a_1 &= -2+\mu\big[b_1+b_2+(y_1-y_2)^2 \\ &\quad -2y_1y_2+\alpha(y_1+y_2)\big]+O(\mu^2) \\ a_2 &= 1-\mu\big[b_1+b_2-(y_1+y_2)^2 \\ &\quad +2y_1y_2+\alpha(y_1+y_2)\big]+O(\mu^2). \end{aligned}$$

Using the definitions of y_1 and y_2, these can be rewritten

$$\begin{aligned} a_1 &= -2+\mu(b_1+b_2)+2\mu(\alpha^2-1) \\ a_2 &= 1-\mu(b_1+b_2). \end{aligned} \tag{2.3.8}$$

Recall that b_1 and b_2 are defined in (2.3.6) in terms of y_1 and y_2. At $\alpha = \pm 1$, $b_1 + b_2 = 0$. The corresponding value of a_2 is 1, indicating that these values are critically stable. In fact, $\alpha < -1$ implies that $b_1 + b_2 < 0$, which demonstrates that the calculated orbit is unstable as a two-periodic orbit. For $\alpha > 1$, $b_1 + b_2$ is greater than 0, indicating that this is a stable two-periodic orbit. Indeed, this explains the behaviors observed in Examples 1 and 2. The first example is within the stability region for the two-periodic orbit, and hence it converges to this orbit. This illustrates the effect of the flip bifurcation at $\alpha = 1 - \mu/2$ in which the stable equilibrium for $0 < \alpha < 1 - \mu/2$ is transformed into a stable two-periodic orbit when $\alpha > 1$. Example 2, by contrast, is in the region where a two-periodic orbit would be unstable. Hence the time behavior cannot converge to this solution. Fig. 5 shows a phase portrait for this example. The two points of the calculated orbit are the tiny x's inside the two fuzzy ovals. The trajectories jump from oval to oval at each iteration. This is the effect of crossing the Hopf bifurcation at $\alpha = -1$. We will have more to say about this figure later on.

How large can α get and still retain stability of this two periodic orbit? for $\alpha \gg 1$, $y_1 \sim \alpha + 1/2$, $y_2 \sim 1/2$, and hence $b_1 + b_2$ is approximately $3/4\alpha$. When a_1 of (2.3.8) becomes larger than 2, then the roots of the characteristic polynomial will have magnitude larger than unity. This occurs when

$$\alpha^2 + 3/8\alpha - 2/\mu > 0. \tag{2.3.9}$$

For $\mu = 0.01$ (as in Examples 1 and 2), this gives $\alpha \sim 14$. Simulations show a bifurcation point at $\alpha = 13.8$, when a four-periodic orbit comes into existence. We suspect that this is the beginning of a period doubling sequence leading into chaos, as suggested by the simulations in Fig. 11. Physically, this can be interpreted as a violation of the "small stepsize" assumption. Note that as μ is decreased, (2.3.9) implies that the two periodic sequence remains stable for larger and larger α.

The stepsize induced instabilities of the previous paragraph for large α are a result of the way the system has been parameterized. If $\alpha = \beta v/w$ assumes a large value by w being very small, then $\mu = \mu'/w^2$ must be large. In order to investigate the system for vanishing w and small stepsize, consider the following alternate parameterization of (1.3)–(1.4), where $v_k = v$ and $w_k = w$ are again assumed constant. Using $\tilde{\mu} = \mu'\beta^2 v^2$, $g_k = \beta\tilde{h}_k$, $z_k = x_k/\beta v$, and $\gamma = w/\beta v$, this is

$$G\begin{pmatrix} z \\ g \end{pmatrix} = \begin{pmatrix} zg+\gamma+1 \\ g-\tilde{\mu}z^2 g-\tilde{\mu}z \end{pmatrix}. \tag{2.3.10}$$

Small γ correspond to small w. In fact, γ is the inverse of α, and we can consequently investigate the behavior of the system for infinite α by investigating (2.3.10) for γ near 0. Mimicking the analysis for F, we find

$$DG(z,g) = \begin{pmatrix} g & z \\ -2\tilde{\mu}zg-\tilde{\mu} & 1-\tilde{\mu}z^2 \end{pmatrix}. \tag{2.3.11}$$

When $\gamma \neq 0$, there is an equilibrium at $z = \gamma$, $g = -1/\gamma$,

which has characteristic equation $s^2+(1/\gamma-1+\tilde{\mu}\gamma^2)s-1/\gamma$, indicating instability for $|\gamma|<1$. At $\gamma=0$, there is no finite equilibrium, but there is a two-periodic orbit, which alternates between $(-1,1)$ and $(-1,0)$. For small but nonzero γ, there is a two-periodic orbit at

$$g_1=-1+O(\gamma^2)$$
$$g_2=-1+(\tilde{\mu}/2\gamma)+O(\gamma^2)$$
$$z_1=1+\gamma/2+O(\gamma^2)$$
$$z_2=\gamma/2+O(\gamma^2).$$

The stability of this orbit can be investigated easily using (2.3.11), that is, $DG^2(z_1,g_1)=DG(z_2,g_2)DG(z_1,g_1)$, which gives

$$\begin{pmatrix}1-\tilde{\mu} & 1\\ \tilde{\mu}^2-2\tilde{\mu}-\gamma+\tilde{\mu}\gamma+0.5\tilde{\mu}^2\gamma & 1-\tilde{\mu}-0.5\tilde{\mu}\gamma\end{pmatrix}+O(\gamma^2). \tag{2.3.12}$$

The characteristic equation of (2.3.12) is then $s^2+a_1s-a_2$ where

$$a_1=-2+2\tilde{\mu}+\frac{\tilde{\mu}\gamma}{2}+O(\gamma^2)$$
$$a_2=1+\gamma\left(1-\frac{3\tilde{\mu}}{2}\right)+O(\gamma^2). \tag{2.3.13}$$

Consequently, for small positive γ, (and $\tilde{\mu}<2/3$), the two-periodic orbit is stable, while for small negative γ, the orbit is unstable. The $\gamma=0$ point, with $a_1=1$ and $a_2=-2+2\tilde{\mu}$, is a nondegenerate Hopf bifurcation, since the eigenvalues cross the unit circle close to (but not at) the -1 point.

III. The Averaged System

The behavior of the adaptive hybrid model (1.5) can be analyzed for more general input signals using nonlinear averaging theory as in [9], simplifying and extending the analysis in [12]. This approach defines an averaged equation which holds for small μ on a timescale of $O(1/\mu)$, to which the behavior of the full system can be compared. The averaged equation is examined for inputs which have a spectral density, and two examples are given. In the steady-state case the averaged analysis is less precise than the analysis of Section 2.3 but estimates of the region of attraction are obtained. When the inputs are sinusoidal, conditions on the relative magnitudes and frequencies of the inputs are derived which ensure the existence of a stable operating averaged equilibrium. Failing these conditions, the averaged equation (and hence the hybrid system itself) will leave the stability region, causing the bursting behavior.

Consider (1.5) with given initial conditions y_0 and h_0, and define $x_{k+1}^*(h)$ for $|h|<1-\epsilon$ where $1\gg\epsilon>0$ as

$$x_{k+1}^*(h)=hx_k^*(h)+v_k+w_k \tag{3.1}$$

with $x_0^*=y_0$. By introducing $z_k=y_k-x_k^*(h)$ (with $z_0=0$), (3.1) and the first line of (1.5) can be shifted to the origin as

$$z_{k+1}=z_kh_k-x_k^*(h_k)(h_{k+1}-h_k)-h_k\int_{h_k}^{h_{k+1}}\frac{dx^*(h)}{dh}\,dh \tag{3.2}$$

where the integral expresses the difference between $x_k^*(h_{k+1})$ and $x_k^*(h_k)$. The second line of (1.5) then becomes

$$h_{k+1}=\left(1-\mu(z_k+x_k^*(h_k))^2\right)h_k-\mu v_k(z_k+x_k^*(h_k)). \tag{3.3}$$

Note that $x_k^*(h)$ and $(D_hx^*(h))_k$ are bounded whenever v_k and w_k are bounded and $|h|<1-\epsilon$. If x_0 and $x_k^*(h)$ are $O(1)$, then z_k of (3.2) is $O(\mu)$. Thus as long as $|h_k|<1-\epsilon$, (3.3) can be rewritten

$$h_{k+1}=\left(1-\mu x_k^*(h_k)^2\right)h_k-\mu v_kx_k^*(h_k)+O(\mu^2). \tag{3.4}$$

Consequently, the loop gain h_k of the adaptive hybrid system (1.5) can be approximated up to first order in μ over the timescale $O(1/\mu)$ by the averaged equation

$$h_{k+1}^*=(1-\mu f(h_k^*))h_k^*-\mu g(h_k^*) \tag{3.5}$$

provided $|h_k^*|<1-\epsilon$. The error made in the averaging process is $|h_k-h_k^*|=O(\delta(\mu))$ over a timescale of $O(1/\mu)$, where $\delta(\mu)$ is an order function in μ. Hence the system loop gain h_k remains in $D=(-1+\epsilon,1-\epsilon)$ as long as h_k^* remains in $D^*=(-1+\epsilon+\delta(\mu),1-\epsilon-\delta(\mu))$. In principle, it is possible to do a little better, with x_0 in a domain of $O(1/\mu^\alpha)$ for $0\leqslant\alpha<1$, which gives z_k as $O(\mu^{1-\alpha})$. This yields the same averaged equation, but with a worse $\delta(\mu)$ for the $h_k-h_k^*$ approximation.

If f and g cause (3.5) to have an attractive fixed point in D^*, then the timescale can be extended to infinity. On the other hand, one expects that if h_k^* eventually leaves D^*, then h_k will also leave D, and instability will result, at least locally. If h_k^* has an attractor outside D^* (and none inside), then h_k will also be driven from D. In short, the behavior of the averaged system (3.5) reflects the behavior of the whole system. For certain classes of f and g, it is possible to explicitly verify these assertions.

3.1. Steady State Revisited

To understand the advantages (and limitations) of this averaging approach, consider again the case of dc signals. With $v_k=v$ and $w_k=w$ for all k, (3.1) can be iterated to obtain

$$x_k^*(h)=h^kx_0+\frac{v+w}{1-h}+O(h^k). \tag{3.6}$$

For $|h|<1-\epsilon$, the steady-state convergent solution is $x^*=(v+w)/(1-h)$. For x_0^* which are $O(1)$ (and consequently for z_k which are $O(\mu)$), and following the logic of (3.2) to (3.5), the loop gain h_k can be approximated to first order in μ over the timescale $O(1/\mu)$ by

$$F(h)=\left(1-\mu\left(\frac{v+w}{1-h}\right)^2\right)h-\mu\frac{v(v+w)}{1-h}. \tag{3.7}$$

The fixed point $h^*=-v/w$ is stable if v and w are such that $|v/w|<1-\epsilon$ and if $\mu<2/x^{*2}$. (A consistent choice for the approximation error made in the averaging process is $\epsilon=\delta(\mu)=\mu^{1/3}$).

Fig. 6 plots $F(h)$ versus h giving a vivid picture of the dynamics of (3.7) for v and $w>0$. Initializing h_0 to the left of $1-\epsilon$, the map iterates down towards the equilibrium $-v/w$. If the mapping is initialized to the left of $-v/w$, then the value of h is increased. Thus, for $-v/w$ and h_0 in $(-1,1-\epsilon)$, the system converges to its equilibrium. Overall, in this simple dc case, the analysis is less precise than the

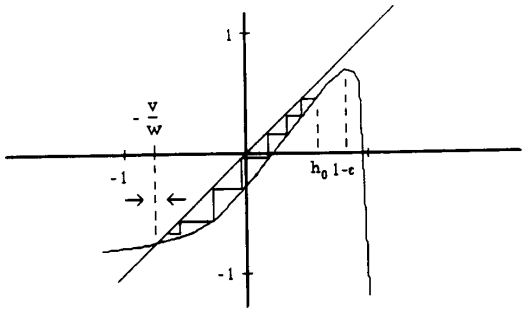

Fig. 6. Region of attraction $v, w > 0$.

direct methods of Section II, but it gives a good approximation to the region of attraction of the equilibrium, something obtainable by no other method (of which we are aware).

3.2. General Inputs

The averaged equations (3.1) and (3.5) can be used to evaluate the behavior of the adaptive hybrid whenever the inputs v_k and w_k have a spectral density. For a given h, (3.1) is a linear time invariant system with input $v_k + w_k$, and its power spectrum is readily expressed in terms of its transfer function and the spectrum of the inputs. Parseval's theorem can then be used to evaluate the averages of f and g in (3.5) as

$$f(h) = \frac{1}{2\pi}\int_{-\pi}^{\pi} \frac{1}{|e^{jw}-h|^2}|V(jw)+W(jw)|^2\,dw$$

$$g(h) = \frac{1}{2\pi}\int_{-\pi}^{\pi} \frac{1}{|e^{jw}-h|}V(jw)(V(jw)+W(jw))\,dw \quad (3.8)$$

If, in addition, the two inputs are uncorrelated (have different support in the frequency domain), then the cross terms in (3.8) average to zero, and

$$f(h) = \frac{1}{2\pi}\int_{-\pi}^{\pi} \frac{1}{|e^{jw}-h|^2}\left(|V(jw)|^2+|W(jw)|^2\right)dw$$

$$g(h) = \frac{1}{2\pi}\int_{-\pi}^{\pi} \frac{1}{|e^{jw}-h|}|V(jw)|^2\,dw. \quad (3.9)$$

Such decorrelation is quite reasonable in view of the application. Note that f and g are well defined and differentiable whenever $|h| \neq 1$. The equilibrium of the averaged system (3.5) are then solutions of

$$\boldsymbol{F}(h) = hf(h) + g(h) = 0. \quad (3.10)$$

Combining (3.9) with (3.10) gives the equilibria of the system as those values of h for which

$$\boldsymbol{F}(h) = \frac{1}{2\pi}\int_{-\pi}^{\pi} \frac{h|W(jw)|^2}{|e^{jw}-h|^2} + \frac{e^{-jw}|V(jw)|^2}{|e^{jw}-h|^2}\,dw = 0. \quad (3.11)$$

Suppose there are $\underline{h}$ and $\bar{h}$ such that

$$-1+\epsilon < \underline{h} < \bar{h} < 1-\epsilon \text{ with } \boldsymbol{F}(\underline{h}) > 0 \quad \text{and} \quad \boldsymbol{F}(\bar{h}) < 0 \quad (3.12)$$

then the averaging is valid and the solutions are well defined. Thus there is an h with $\underline{h} < h < \bar{h}$ such that (3.10) holds. The interval $(\underline{h}, \bar{h})$ is invariant under the flow of the averaged system for sufficiently small μ, and there is at least one stable averaged equilibrium. For μ small enough, and with appropriate initial conditions, the system will converge to a region about this averaged equilibrium.

Of course, (3.11) may well have solutions outside $(-1,1)$ (and none inside). The system will then leave $(-1,1)$ along with the averaged equation, resulting in local instability and "bursts". When the averaged system leaves $(-1,1)$ due to an attractor outside this set, the time between bursts can be estimated. Assume h_0^* is uniform in $(-1,1)$ and compute the time k^* at which $h_{k^*}^*$ is 1 or -1. These times k^* can then be averaged over all h_0^* to give the mean time between bursts. This average is on the order of $1/\mu$ with an error of $O(1)$. This estimate agrees well with the observations in [3] that the rate of drift toward instability is essentially linear in the stepsize.

Note that if the distribution of V is symmetric with respect to $\pi/2$ on $(0,\pi)$, then $\boldsymbol{F}(h)$ reduces to just the first term under the integral in (3.11). This has exactly one zero at $h = 0$, and consequently the hybrid will always work, that is, $h_k \to O(\mu)$ as k goes to infinity for suitably small h_0 and μ.

3.3. Sinusoidal Inputs

As evidence of the ease of application of (3.11), consider the case of sinusoidal inputs $v_k = V\cos\alpha k$, $w_k = W\cos\beta k$ with $0 < \alpha < \pi$, $0 < \beta < \pi$ and $\alpha \neq \beta$. The functions $f(h)$ and $g(h)$ can be readily calculated to give $\boldsymbol{F}(h)$ of (3.11). Using pole–zero techniques it is possible to verify that $\boldsymbol{F}(h) = 0$ has only one real root, which belongs to $(-1,1)$ if and only if

$$0 < \frac{V^2}{W^2} < \frac{\cos\alpha+1}{\cos\beta+1}\cdot\frac{1}{\cos\alpha} \quad (3.13)$$

for $\cos\alpha > 0$, and

$$0 < \frac{V^2}{W^2} < \frac{\cos\alpha-1}{1-\cos\beta}\cdot\frac{1}{\cos\alpha}$$

for $\cos\alpha < 0$. When (3.13) holds, $\boldsymbol{F}(1) > 0$ and $\boldsymbol{F}(-1) < 0$, which demonstrates stability of the equilibrium and gives the region of attraction as $(-1,1)$. This extends the analysis of [12] in a form which is easily generalizable to higher dimensional problems, and also gives a valuable expression for the domain of attraction of the equilibrium. One might also extend these basic averaging results to consider almost periodic inputs (as in [18]), though we have not pursued this avenue here.

IV. The Pictures...

The analysis of the previous sections has brought us to the point where we can give a fairly complete explanation of the global behavior of the single parameter adaptive hybrid. Consider Fig. 7. For $|\alpha| < 1$, there is a unique stable equilibrium. At $\alpha = 1$ there is a flip bifurcation (equation (2.2.5)) that sheds a two periodic orbit, which is initially stable (2.3.7)–(2.3.8). At about $\alpha \sim 13.85$, there is another bifurcation, with the exact value of the parameter dependent on the value of μ ($\mu = 0.01$ was used). The two periodic orbit becomes unstable and a stable four-periodic orbit is formed. At around $\alpha > 14.36$, instabilities due to the stepsize over-

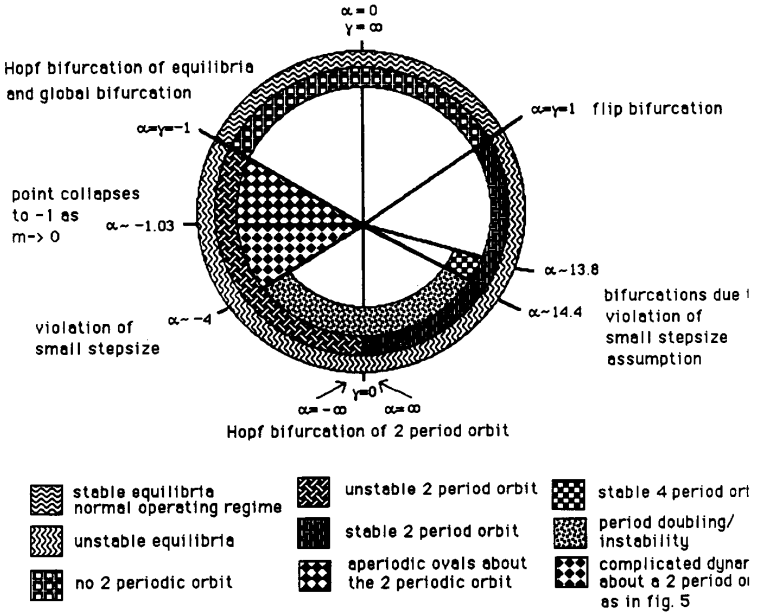

Fig. 7. Bifurcation diagram for adaptive hybrid parameterized by α and γ.

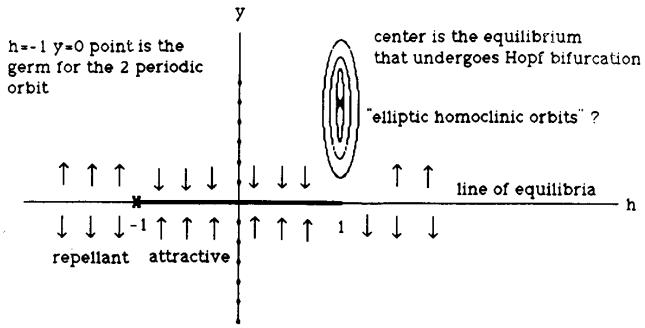

Fig. 8. Global bifurcation point at $\alpha = -1$.

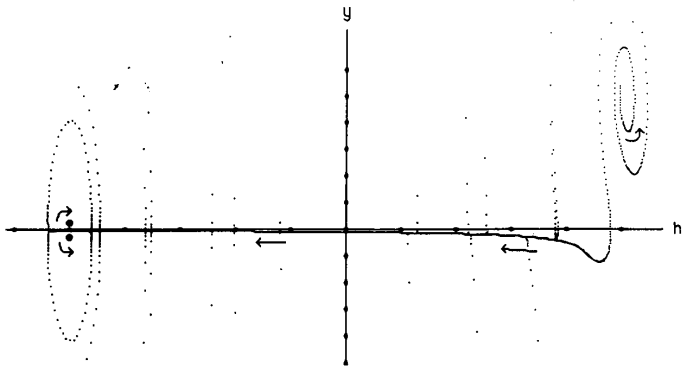

Fig. 9. Phase portrait for $\alpha = -1.02$.

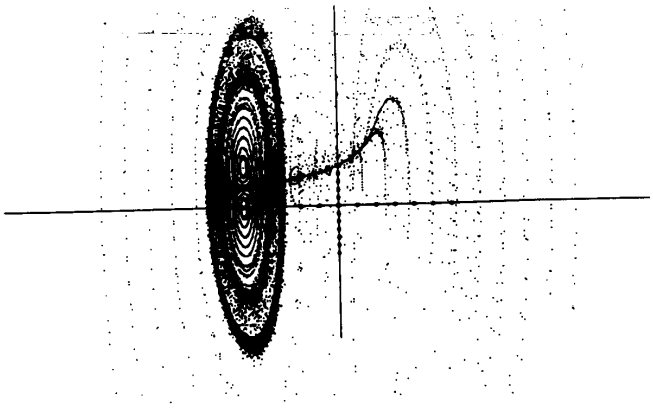

Fig. 10. Multiple phase portraits for $\gamma = 0$.

whelm the system, and we lose the ability to track the behavior.

In the negative direction, the behavior is considerably more complex. The point at $\alpha = -1$ is a global bifurcation point. With respect to the equilibria (2.2.3), the Jacobian can be written

$$\begin{pmatrix} h^* & 0 \\ -\mu\alpha & 1 \end{pmatrix} \tag{4.1}$$

which has eigenvalues at 1 and h^* for any h^*. Thus the subspace $y^* = 0$ is attractive for $|h^*| < 1$, and repellant for $|h^*| > 1$.

Fig. 8 gives a graphic interpretation of the behavior of the phase trajectories of the system at this global bifurcation point. In the left half plane, the trajectories bounce from top to bottom at alternate iterations, eventually flowing into one of the attractive points at $y^* = 0$ and $|h^*| < 1$. In the right half plane, trajectories move straight to the $y^* = 0$ line or they become trapped about the equilibrium at (1,1). The $h = -1$ point is the germ that starts the two periodic orbit that later undergoes a Hopf bifurcation. The $h = 1$, $y = 1$ point is the fixed point analyzed above which undergoes a Hopf bifurcation and is the origin of the stable aperiodic orbits seen for α near -1.

As α crosses the -1 bifurcation point, several things happen. Compare Fig. 8 with Fig. 9, which shows a phase portrait of several trajectories for $\alpha = -1.02$. First, the equilibrium becomes unstable (as shown in (2.2.5)) and the surrounding orbits become unstable. This is pictured in the outward spiral in the upper right-hand corner of Fig. 9. Note that the arrows have been added to the simulation to indicate the general direction of motion. Second, the $y = 0$, $h = -1$ point splits into an unstable two periodic orbit (as demonstrated in (2.3.7)–(2.3.8)). These are the small x's inside the small circles near the $h = -1$ point. Most likely, the circles themselves are stable aperiodic orbits. Third, the subspace of equilibria disappears, and is replaced by a long, slowly moving trajectory that channels the right half plane trajectories to the aperiodic orbit near $h = -1$. This can be explained by the averaging analysis of Section III. The "linear" drift corresponds to the slow motion of $x^*(h_k)$ of (3.1) for small μ. Such a long slow funneling trajectory is thus expected (and encountered in simulations) for more general inputs as well.

As $|\alpha|$ increases further (a small amount that appears to go to zero as the stepsize μ vanishes), the aperiodic orbits grow larger, until at $\alpha \sim 1.04$ (for $\mu = 0.01$) the touch. At this point, the aperiodic orbit appears to become unstable, and the behavior of Fig. 5 appears. This simulation was begun after 25 million iterations...; one can only suppose that the tattered edges of this figure are not transients that will die away, but rather are in intrinsic feature of its behavior.

It is fair to say that we do not have a detailed understanding of this region in parameter space. We observe aperiodic orbits, and p-periodic orbits for just about any p. For instance, at $\alpha = -10$ and $\mu = 0.001$ there is a stable 108 periodic orbit. At $\alpha = -29$ (and $\mu = 0.001$) there is a stable 18 periodic orbit existing simultaneously with an aperiodic orbit (but with different regions of attraction, with a possibly fractal boundary). We are unsure how to classify Fig. 5, though it does provide a pictorial explanation of the "bursting" phenomena in adaptive hybrids.

In [3], bursting was described as non-periodic, yet repetitive. It appeared bounded, yet it never "settled down" to any limit cycle. The bursting behavior consists of a long linear drift phase (the horizontal segment just below the h axis), followed by a "short" wildly oscillating phase (where in a handful of iterations the y values oscillate to large values, and then just as rapidly "restabilize"). If one plots Fig. 5 as the h value verses time instead of in the phase plane, the graph is nearly identical to the plots in [3].

Moreover, it is easy to see that as α decreases (gets larger in magnitude) the underlying unstable two-periodic orbit grows away from the h axis (from (2.3.4) and (2.3.6)). This causes the unstable aperiodic orbit to increase, and hence the magnitude of the fuzzy ovals in Fig. 5 increases. Since α is the ratio of the two inputs, this essentially ties the *magnitude* of the bursts to the *disparity* of excitation. In adaptive systems terminology, where the input to the adaptive element is called the "excitation" and the input that appears directly in the error term r_k (recall Fig. 2) is considered the "disturbance," one says that the degree of excitation (the ratio of these two terms, in our case, α) is insufficient to guarantee stability of the algorithm. The present dynamic analysis suggests that such a degree of excitation condition is

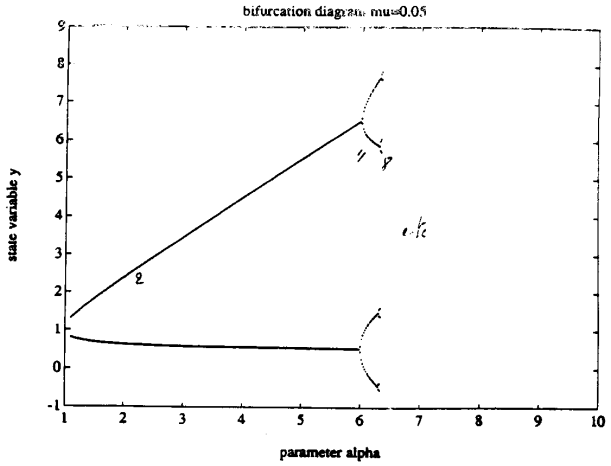

Fig. 11. Bifurcation diagram showing period doubling.

virtually necessary in order to avoid undesirable behaviors such as the strange "bursting" of Fig. 5. The averaging analysis shows that magnitude alone is not enough to specify the true "region of stability," and that frequency effects must also be taken into account. In particular, signals which are uncorrelated have the best chance of avoiding the bursting misbehavior.

Returning to the bifurcation diagram of Fig. 7, note the bifurcations at $\alpha = -4$, 13.8, and 14. These (and the resultant four periodic and unstable behaviors) are due to a violation of the small stepsize assumption (as shown in (2.3.9)) caused by the form of our parametrization of μ as μ'/w^2. By reparametrizing the system with $\alpha = 1/\gamma$, it is possible to sidestep the small μ issue, and to examine the behavior for α near (and at) infinity. This was, in fact, the case analyzed in [3]. The $\gamma = 0$ (α = infinity) point is shown to be a nondegenerate Hopf bifurcation (2.3.13), where the two periodic orbit changes from stable ($\gamma = 0^+$) to unstable ($\gamma = 0^-$). Fig. 10 shows a multiple trajectory phase portrait of this bifurcation point. The marginally stable two periodic orbit lies in the center of the sets of nested ellipses, surrounded by families of what appear to be aperiodic orbits. The dark "tail" that stretches into the right half plane is a funnel that collects trajectories and feeds them to the aperiodic orbits (representing x^* of the averaged equation). This diagram suggests that there will likely be a great deal of sensitivity to initial conditions and to small roundoff (or other) errors, since trajectories close together on the "tail" may well ultimately join very different ellipses. Thus, the qualitative behavior is robust to small perturbations (all trajectories studied ultimately enter one of the ellipses) while the quantitative behavior is susceptible to numerical problems (it is hard to tell *which* ellipse a given starting point will join).

The adaptive hybrid appears to also be susceptible to the period doubling route to chaos, as in Fig. 11. This bifurcation diagram 2, 4, and 8 period orbits for varying values of α (for $\mu = 0.05$). This route to chaos is essentially due to a violation of the small stepsize assumption since μ fails to be always less than $2/y^2$. The domain of attraction of the periodic orbits shrinks rapidly for large values of α, and numerical errors lead to instabilities while simulating. This path has not been pursued in detail.

Overall, we have provided three possible explanations of the observed bursting behavior of the adaptive hybrid. For $\alpha > 1$, the bursting may be a transient phenomena that will eventually decay into a two periodic orbit. For $\alpha < -1$, the bursting may be due to strange dynamics as in Fig. 5. For α at infinity (i.e., $w = 0$), the bursting may be an aperiodic orbit. In the latter two cases, the behavior is not transient and will not die away with time.

V. Conclusions

The simplified model of the adaptive hybrid system has been analysed, leading to the bifurcation chart of Fig. 7. This details the regions of stability and instability of the various equilibria, periodic orbits, aperiodic orbits, etc., that arise from the various types of bifurcations. The strange dynamics of Fig. 5 were identified and seen to arise from a particular degenerate global bifurcation. The adaptive hybrid of (1.5) is one of the simplest known systems which exhibits such complex dynamics, and as such may provide a useful test bed for analysis of this complicated form of nonlinear behavior.

The results may help to explain the "bursting" behavior encountered in adaptive systems such as the hybrid. Depending on the operating conditions, the bursting may resemble a stable periodic orbit, a stable aperiodic orbit, or a more complicated figure such as a strange attractor. These behaviors arise when the normal operating conditions of the adaptive scheme fails, that is, when the ratio of the power of the "input" to the power of the "disturbance" falls below a certain threshold. This can be described as a lack of persistence of excitation.

In surveying the adaptive literature, there have been numerous attempts to both describe and explain the misbehaviors of adaptive systems. The bursting of the adaptive hybrid is chronicled in [3]. In [5], the bursting of an adaptive control scheme is attributed to a lack of persistence of excitation combined with the presence of disturbances inside a feedback loop. In [6], an adaptive infinite impulse response (IIR) identification scheme is shown to undergo repetitive bursts

of destabilization, followed by restabilization. This behavior appears nearly identical to the bursting encountered here, and is extended in [11] to an examination of the chaotic dynamics for large stepsizes. In [4], chaotic behavior of an adaptive regulator is shown when the stepsize is allowed to become large (essentially deadbeat identification), showing a parallel to the breakdown of our analysis using the α parameterization for large α. In [7], periodic solutions are described for adaptive systems in the presence of small periodic forcing terms. Recently [14] and [15], interest has been growing in bifurcation-style analyses of the mechanisms of adaptation.

The above analyses are linked in that the adaptive element lies inside a feedback loop. Though the exact equations change with each application, misbehaviors arise when the excitation conditions fail. For the adaptive hybrid excited by constant inputs, we have classified several types of possible (mis)behavior. We suspect that the problems encountered in all of the above analyses are linked, that it is not a pathology of adaptive control, or of adaptive (IIR) identification that such nonlinear behaviors arise. Rather, such "bursting" is an unavoidable consequence of the use of standard adaptive schemes embedded inside a feedback loop when the excitation conditions fail. In essence, this suggests that the persistence of excitation conditions are virtually necessary to assure that one remains in the "good" operating region, the upper third of the bifurcation pie of Fig. 7.

Acknowledgment

The authors would like to thank J. Kenney of Tellabs Inc. for answering numerous questions about the physical characteristics of adaptive hybrids. They are also indebted to L. Praly of The Ecole Des Mines, Paris, for his insistence that there must be a two-periodic orbit in the adaptive hybrid. This observation sparked much of their analysis.

References

[1] M. L. Honig and D. G. Messerschmitt, *Adaptive Filters: Structures, Algorithms, and Applications*. Kluwer-Academic, 1984.
[2] B. Widrow and S. D. Stearns, *Adaptive Signal Processing*. Englewood Cliffs, NJ: Prentice-Hall, 1985.
[3] W. A. Sethares, C. R. Johnson, Jr., and C. Rohrs, "Bursting in adaptive hybrids," *IEEE Trans. on Comm.*, Aug. 1989.
[4] I. M. Y. Mareels and R. R. Bitmead, "Non-linear dynamics in adaptive control: chaotic and periodic stabilization," *Automatica*, vol. 22, no. 6, 1985.
[5] B. D. O. Anderson, "Adaptive systems, lack of persistency of excitation and bursting phenomena," *Automatica*, vol. 21, May 1986.
[6] M. Jaidane-Saidane and O. Macchi, "Quasi-periodic self stabilization of adaptive arma predictors," *Int. J. Adaptive Contr. and Signal Process.*, vol. 2, no. 1, Mar. 1988.
[7] L. Praly, "Oscillatory behavior and fixes in adaptive linear control: A worked example," in *Proc. 1988 IFAC Workshop on Robust Adaptive Control*, pp. 85–90, Newcastle, Australia, Aug. 1988.
[8] Guckenheimer and Holmes, *Nonlinear Oscillations, Dynamical Systems, and Bifurcations of Vector Fields*. New York: Springer-Verlag, 1983.
[9] J. A. Sanders and F. Verhulst, *Averaging Methods in Nonlinear Dynamical Systems*, New York: Springer-Verlag, 1985.
[10] K. Astrom and B. Wittenmark, *Computer-Controlled Systems*. Englewood Cliffs, NJ: Prentice Hall, 1984.
[11] O. Macchi and M. Jaidane-Saidane, "Adaptive IIR filtering and chaotic dynamics: application to audiofrequency coding," *IEEE Trans. Circuits Syst.*, vol. 36, pp. 591–599, Apr. 1989.
[12] Z. Ding, C. R. Johnson, Jr., and W. A. Sethares, "Frequency dependent bursting in adaptive echo cancellation and its prevention using double talk detectors," *Int. J. Adaptive Contr. Signal Process.*, vol. 4, pp. 219–236, 1990.
[13] Golubitsky and Schaeffer, *Singularities and Groups in Bifurcation Theory*. New York: Springer-Verlag, 1985.
[14] M. P. Golden and B. E. Ydstie, "Parameter drift in adaptive control systems: bifurcation analysis of a simple case," *Int. J. Adaptive Contr. and Signal Process.*, to be published.
[15] G. J. Rey, R. R. Bitmead, and C. R. Johnson, Jr., "The dynamics of bursting in simple adaptive feedback systems," *IEEE Trans. Circuits Syst.*, to be published.
[16] B. A. Huberman and E. Lumer, "Dynamics of adaptive systems," *IEEE Trans. Circuits Syst.*, vol. 37, pp. 547–550, Apr. 1990.
[17] J. Kenney, Tellabs Inc., private communication.
[18] B. D. O. Anderson, et al., *Stability of Adaptive Systems: Passivity and Averaging Analysis*. Cambridge, MA, MIT Press, 1986.
[19] I. M. Y. Mareels and R. K. Boel, "A performance oriented analysis of a double hybrid adaptive echo cancelling system," *Syst. and Contr. Theory*, to be published.

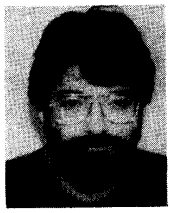

William A. Sethares (S'84–M'87) received the B.A. degree in mathematics from Brandeis University, Waltheim, MA, and the M.S. and Ph.D. degrees in electrical engineering from Cornell University, Ithaca, NY.

He has worked at the Raytheon Company as a Systems Engineer and is currently with the Department of Electrical and Computer Engineering, University of Wisconsin, Madison. His research interests include adaptive systems in signal processing, communications, and control.

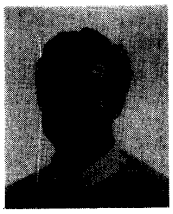

Iven M. Y. Mareels (S'86–M'86) received the B.E. degree in electrical and mechanical engineering from the University of Gent, Gent, Belgium, in 1982, and the Ph.D. degree in systems engineering from the Australian National University, Canberra, Australia, in 1987.

He is currently a senior lecturer at the Electrical Engineering Department of the Australian National University, Newcastle, Australia. His main research interests are focuses on dynamical aspects of systems in signal processing, adaptive control, adaptive identification, power systems, and nonlinear control theory. He is an Associate Editor for *Automatica*, in the area of adaptive control and identification.

Dr. Mareels is a member of SIAM.